Wyznaczanie absolutnych obfitości plazmy rozbłysków słonecznych

Barbara Sylwester, CBK PAN

Referencje

- Measurements of absolute abundances in solar flares; Harry P. Warren, 2014, ApJ, 786, L2
- Solar flare composition and thermodynamics from RESIK X-ray spectra; B. Sylwester, J. Sylwester, K. J. H. Phillips, A. Kępa, and T. Mrozek, 2014, ApJ, 787, accepted
- Plasma composition in a sigmoidal anemone active region; D. Baker, D. H. Brooks, P. Demoulin, L. van Driel-Gesztelyi, L. M. Green, K. Steed, and J. Carlyle; 2013, ApJ, 778, 69

Measurements of absolute abundances in solar flares; Harry P. Warren, 2014, ApJ, 786, L2

EUV Variability Experiment (**EVE**) on **SDO**→ high temp. emission lines (Fe XV-Fe XXIV) &
continuum from thermal bremsstrahlung (proportional to H abundance).
Comparison of relative intensities allows to determine enrichment of flare plasma relative to the composition of photosphere: FIP bias (***f***).
Multiple EUV Grating Spectrograph A (MEGS-A)→ 50-370 Å ; used **60 - 200 Å** (resolution 1Å, cadence 10s.)
21 most intense flares, spectra integrated for each 120 s where *GOES* 1-8 Å flux is ≥M1 level → 640 spectra, pre-flare spectra subtracted
Correction for unknown (or with no reliable atomic data) emission lines formed near ~1MK: multiply pre-flare spectrum by the normalized irradiance of Fe IX 171.07 Å line.

EVE spectrum and *GOES* observations

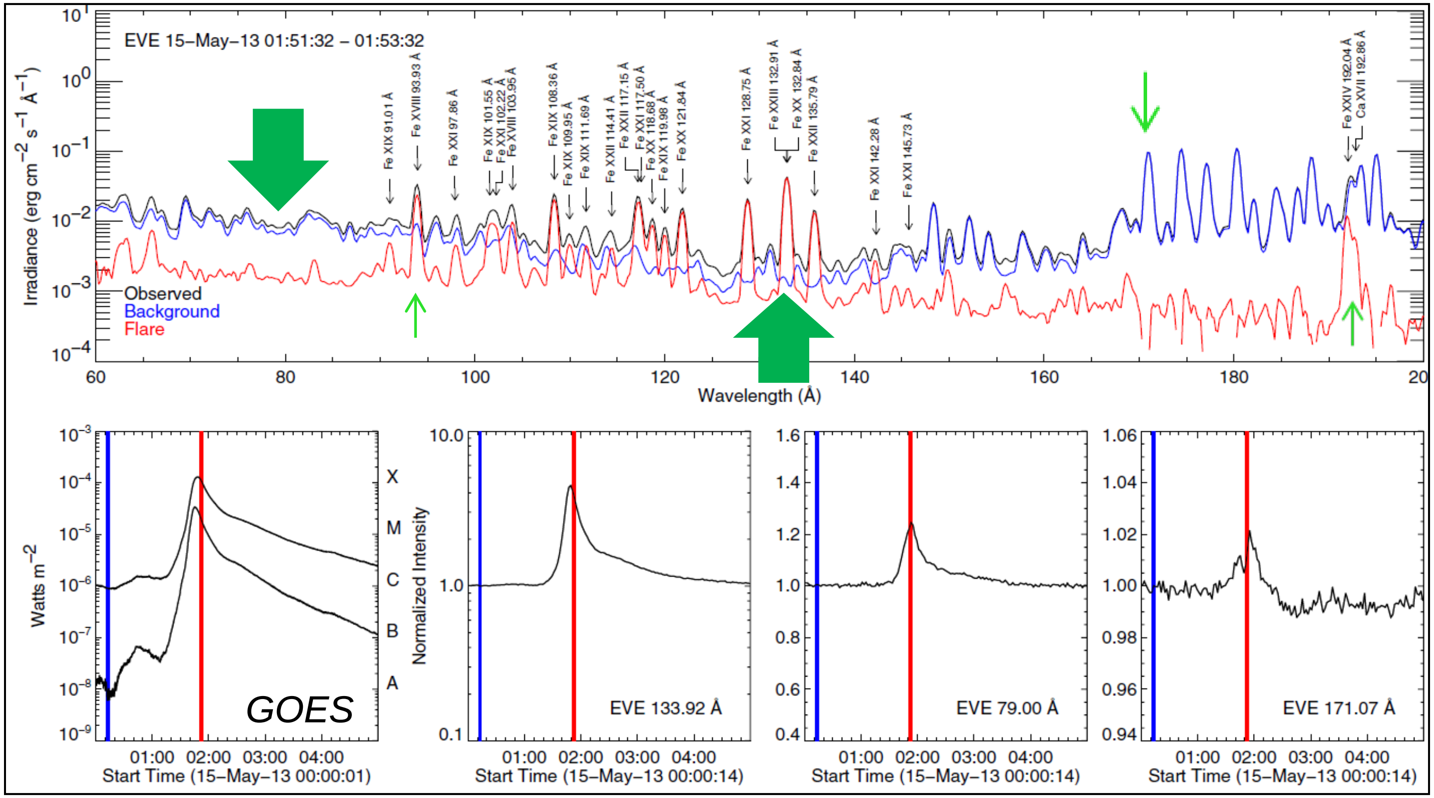

X1.2 flare on 2013 May15: Observed, assumed background and inferred flare irradiance:
~79 Å is predominately continuum
~133 Å emission dominated by Fe XXIII

GOES and EVE light curves for this event: the background radiation is assumed to be the pre-flare irradiance × the normalized EVE 171 Å intensity.

emissivities for unit EM for photospheric composition

1. An isothermal model

f ≡ FIP bias

$$I(\lambda) = \frac{A}{R^2}\left[f\epsilon_L^P(\lambda, T_0)\mathrm{EM}_0 + \epsilon_C^P(\lambda, T_0)\mathrm{EM}_0\right]$$

Line ratios Fe XXIII/Fe XXII (~133 Å)→
T and $\mathrm{EM}_0' = f \times \mathrm{EM}_0$

$$I(\lambda) = \frac{A}{R^2}\left[\epsilon_L^P(\lambda, T_0)\mathrm{EM}_0' + \epsilon_C^P(\lambda, T_0)\frac{\mathrm{EM}_0'}{f}\right]$$

2013 May 15 X1.2 flare (isothermal)

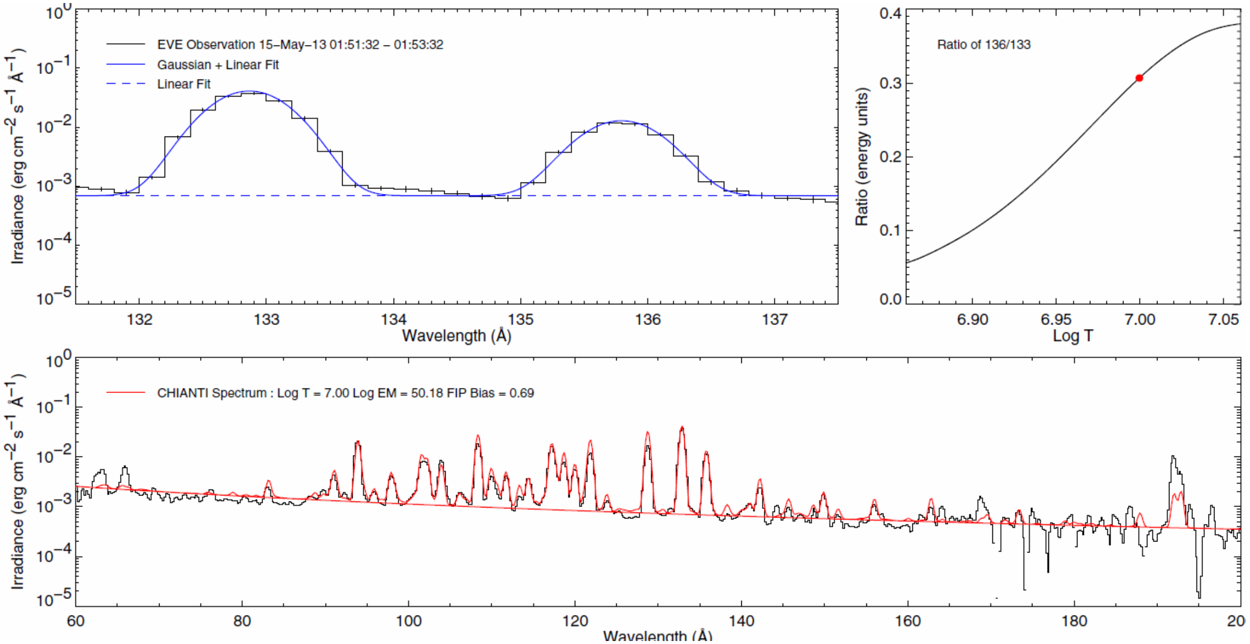

T & EM → Synthesize the expected continuum **Comparison of observed and computed continuum** → FIP bias parameter ***f=0.69***

Add the line and cont. → expected EUV spectrum; Reasonable fit to the line and continuum; the spectrum was taken during the flare decay. Repeated for 21 flares → average ***f*** = 0.85±0.16 which is close to photospheric composition

DEM approach for the same spectrum

$$\xi_V(T_e) = \sum_{k=1}^{N_g} \mathrm{EM}_k \exp\left[-\frac{(\log T_e - \log T_k)^2}{2\sigma_k^2}\right]$$

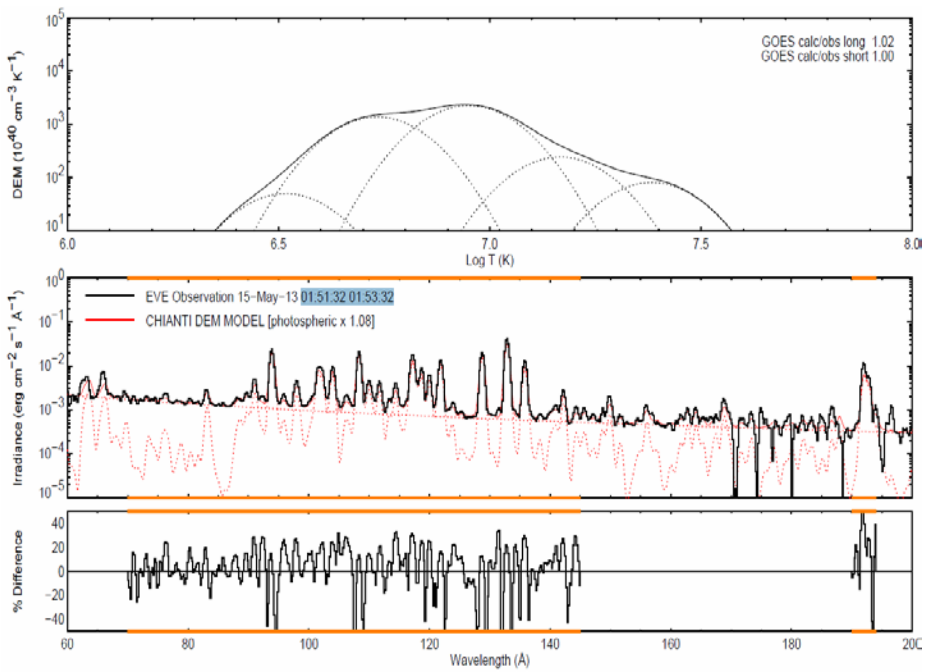

DEM=sum of Gaussians in log space. Number N_g, position ($\log T_k$) and width (σ_k) of Gaussians is fixed for a given calculations and only the magnitude of each component is varied.

Selected initial values for EM_k, f = 1 and use MPFIT (Lovenberg-Marquardt least-square minimization) routine to determine EM components and f that produce the lowest value of χ^2.

→ F =1.08 (close to photospheric)

→ Average for total flare f = 1.26±0.12

Observations of thermal flare plasma with the EUV variability experiment; Harry P. Warren, John T. Mariska, and George A. Doschek, 2013, ApJ, 770,116

Results for two representative events

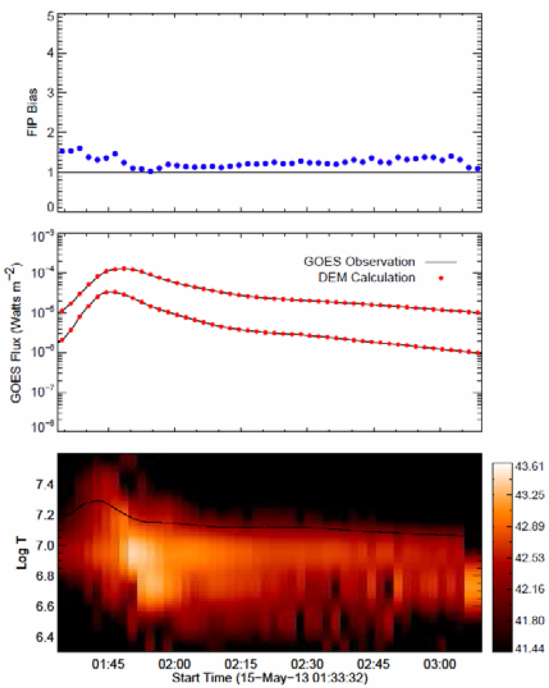

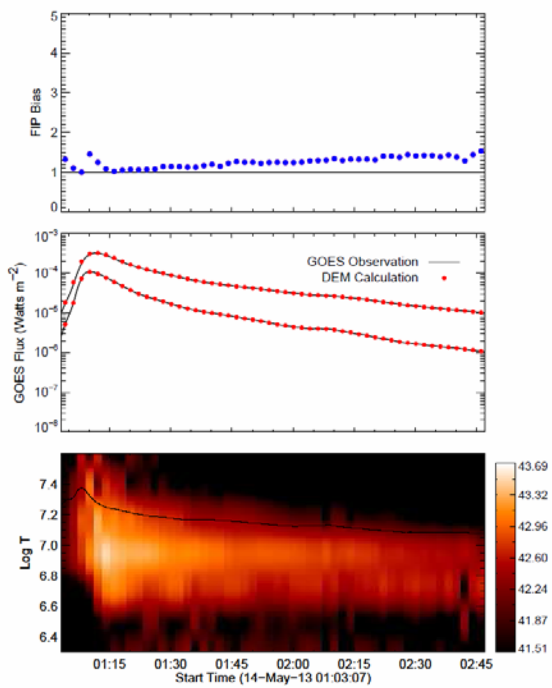

		Isothermal		DEM
Date	Class	T_{start}	f	$f \pm \sigma_f$
09-Aug-11	X6.9	08:21:10	0.97	1.25± 0.14
07-Mar-12	X5.4	00:52:14	0.73	1.25± 0.14
14-May-13	X3.2	01:31:07	0.75	1.25± 0.14
13-May-13	X2.8	16:27:04	0.85	1.11± 0.33
15-Feb-11	X2.2	02:13:21	0.54	1.06± 0.19
06-Sep-11	X2.1	22:35:42	0.75	1.23± 0.22
03-Nov-11	X1.9	20:34:20	1.01	1.38± 0.16
24-Sep-11	X1.9	09:55:24	0.73	1.11± 0.50
23-Oct-12	X1.8	03:27:11	0.94	1.27± 0.14
07-Sep-11	X1.8	22:47:52	0.95	1.24± 0.27
13-May-13	X1.7	02:39:30	0.89	1.26± 0.24
27-Jan-12	X1.7	18:37:41	1.33	1.28± 0.13
09-Mar-11	X1.5	23:27:19	0.98	1.28± 0.14
12-Jul-12	X1.4	17:21:12	0.72	1.36± 0.21
22-Sep-11	X1.4	11:24:33	0.85	1.44± 0.28
07-Mar-12	X1.3	00:52:14	0.73	1.25± 0.14
15-May-13	X1.2	01:51:32	0.69	1.26± 0.12
06-Jul-12	X1.1	23:13:14	0.73	1.19± 0.17
05-Mar-12	X1.1	04:23:29	0.89	1.28± 0.11
04-Aug-11	M9.3	03:59:07	0.83	1.32± 0.15
30-Jul-11	M9.3	02:11:49	0.95	1.37± 0.12

For isothermal model: 21 spectra (a single spectrum for each event selected, during the decay) ***f***=0.84±0.16

For DEM approach: 640 spectra analysed ***f***=1.27±0.23; increase over time for individual events

Evidence that the composition is close to photospheric at all times during a flare.

This result do **NOT** agree with many previous measurements which have indicated an enrichment of a factor 2 or more during flares……but

The ability of DEM model to reproduce the wavelength dependence of the continuum emission from 60 to 200 Å is the most compelling aspect of this analysis.

Solar flare composition and thermodynamics from RESIK X-ray spectra

B. Sylwester, J. Sylwester, K. J. H. Phillips, A. Kępa, and T. Mrozek

ApJ, 2014 accepted

14 Nov. 2002 at 22:26 UT M1.0

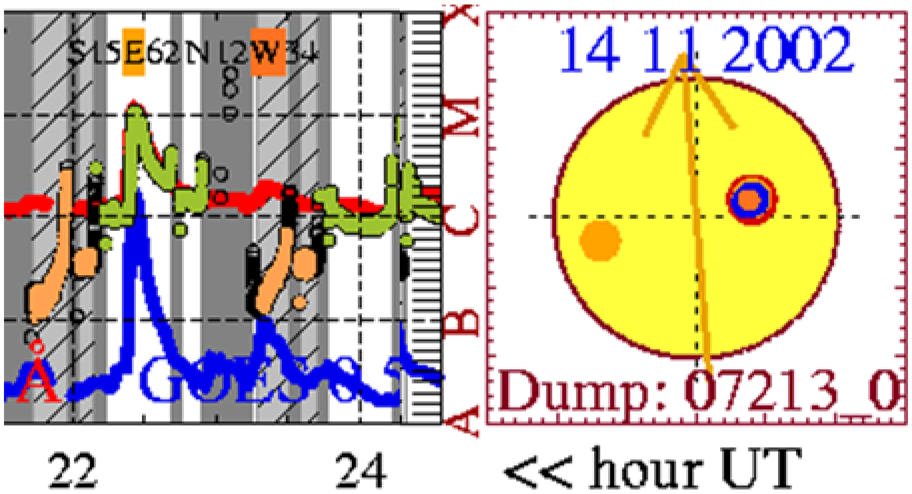

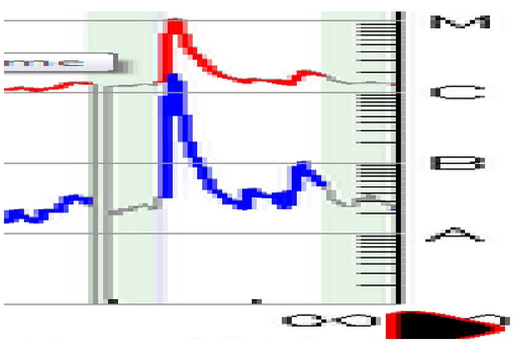

RESIK → 127 widm
RHESSI →~60 obrazów

Hard X-ray impulsive emission

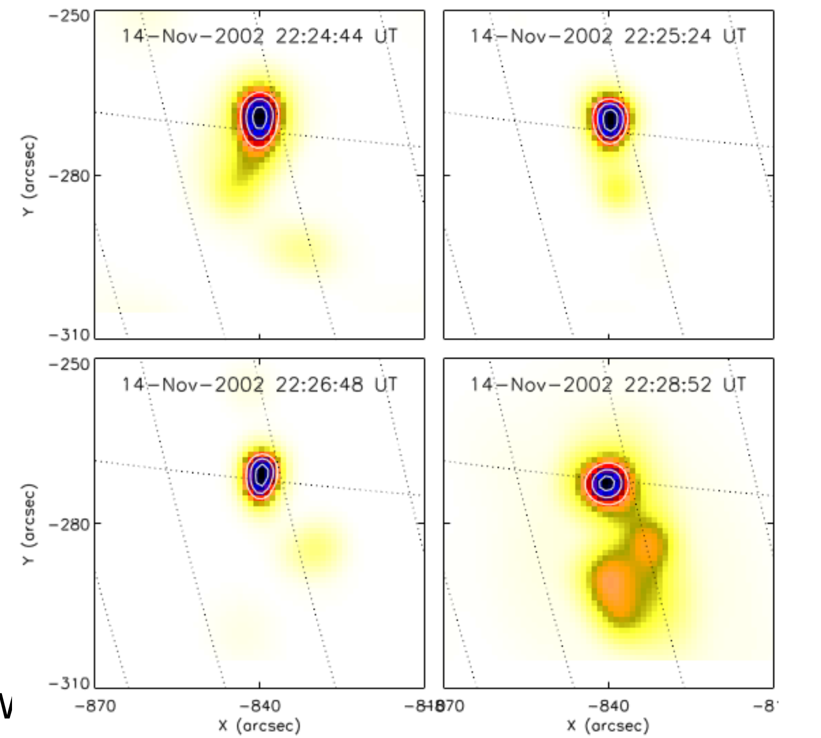

soft X-ray max.

decay

Average RESIK spectrum for M1.0 flare

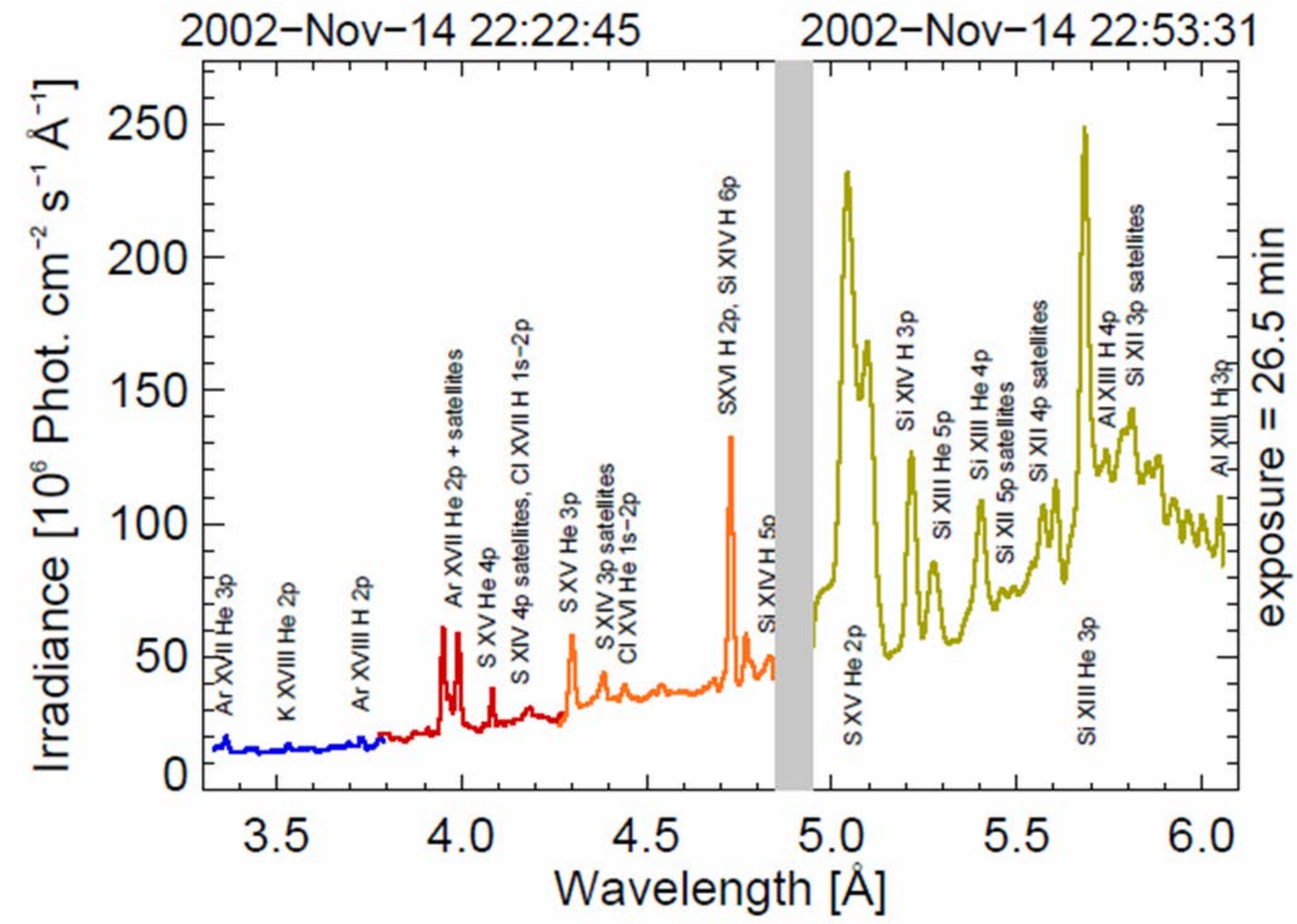

14 Nov. 2002 at 22:26 UT

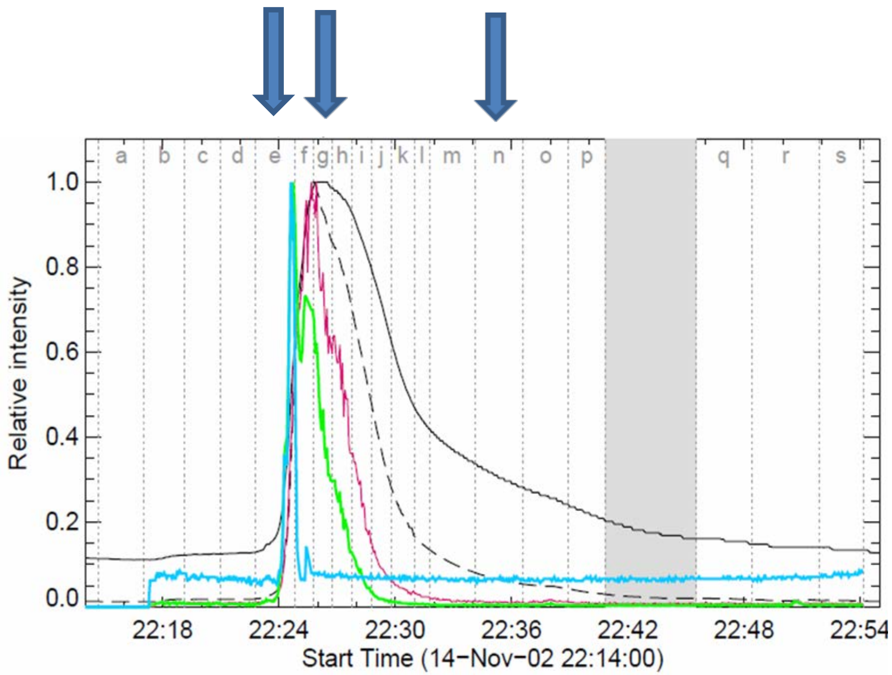

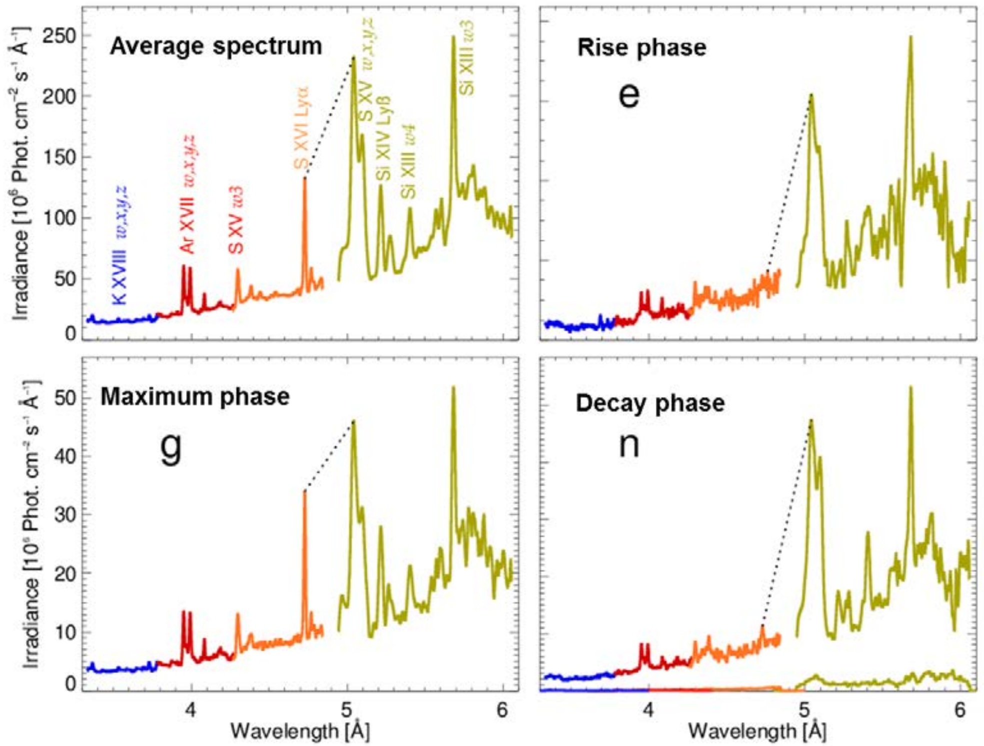

GOES → black

RHESSI → pink (6-12 keV)

green (12-25 keV)

blue (25-50 keV)

DEM vs the abundances

$$F_i = A_i \int_{T=0}^{\infty} f_i(T)\varphi(T)\mathrm{d}T$$

$$DEM \equiv \varphi(T) \equiv {N_e}^2 \frac{\mathrm{d}V}{\mathrm{d}T}$$

Dane: strumienie w 15 przedziałach widmowych zawierających najsilniejsze linie i kontinuum scałkowane po czasie trwania rozbłysku

Strumienie teoretyczne: na podstawie kodu CHIANTI 7.0 zakładając fotosferyczne i koronalne obfitości oraz równowagę jonizacyjną Bryans (ApJ, 691, 2009)

Metoda: Algorytm iteracyjny Withbroe-Sylwester (Solar Phys., 67, 1980)→ 10 000 iteracji do obliczenia DEM oraz 100 realizacji Monte Carlo do wyliczania błędów

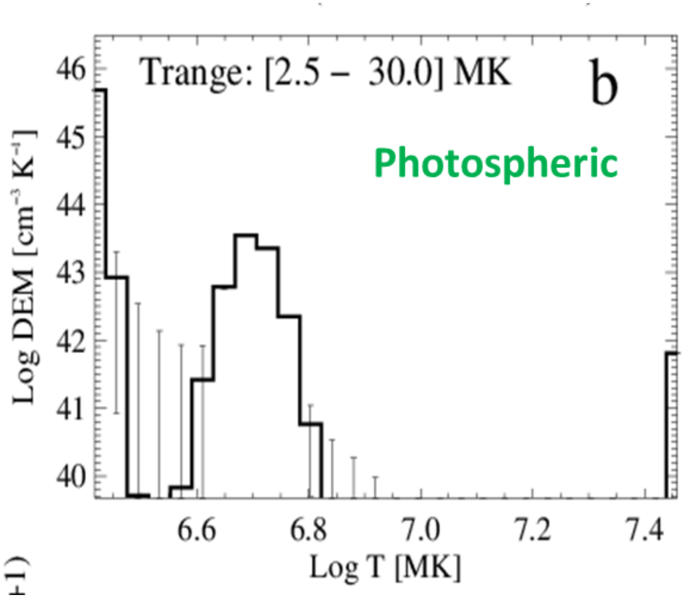

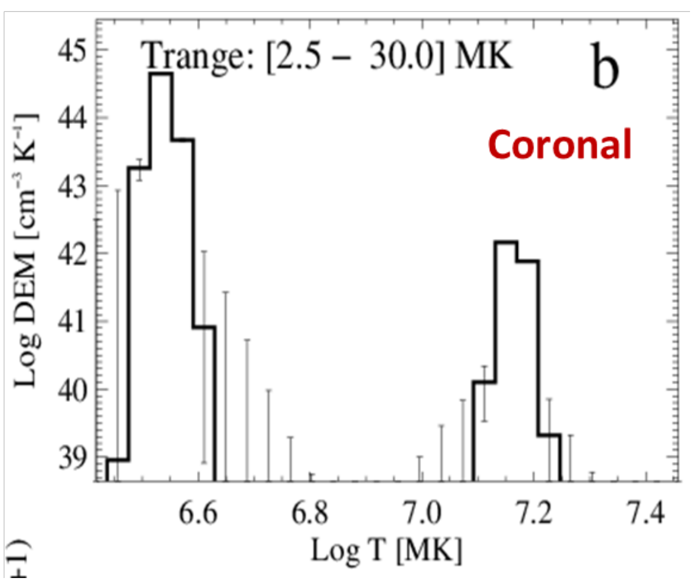

Zakładając różne obfitości otrzymujemy zupełnie różne rozkłady DEM

AbuOpt (for whole spectrum)

$$F_i = A_i \int_{T=0}^{\infty} f_i(T)\varphi(T)\mathrm{d}T$$

for i=1,2…15

Celem jest wyznaczenie obfitości pierwiastka A_i, którego linie są obserwowane w widmie. Rozwiązujemy układ 15 równań wyliczając DEM i zmieniając poszukiwaną wartość A_i zakładając kolejno 21 różnych wartości z przedziału 0.1 - 16 x wartość koronalna (dla pozostałych pierwiastków pozostawiamy wartość koronalną). Dla każdego zestawu strumieni po 1000 iteracjach otrzymujemy: A_i, φ_i, oraz najlepsze dopasowanie χ^2. Badamy zależności A_i vs χ^2. wyznaczamy wartość obfitości, która daje najlepsze dopasowanie widm obserwowanych i wyliczonych z modelu.

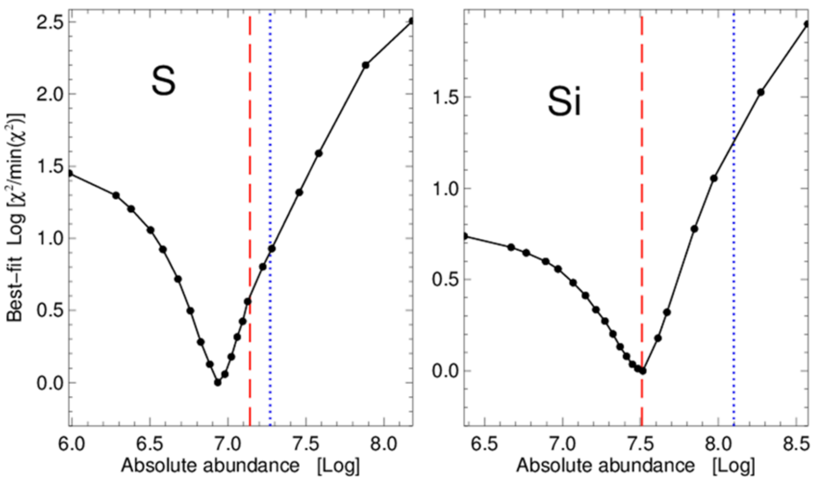

Otrzymane wyniki interpretujemy w ten sposób, ze obfitości odpowiadajace min. χ^2 są optymalne - dla nich zgodność pomiędzy strumieniami obs. i wyliczonymi z modelu jest najlepsza.

Dashed red line denotes the photospheric and dotted blue the coronal abundance.

14 Nov. 2002; for 19 time intervals

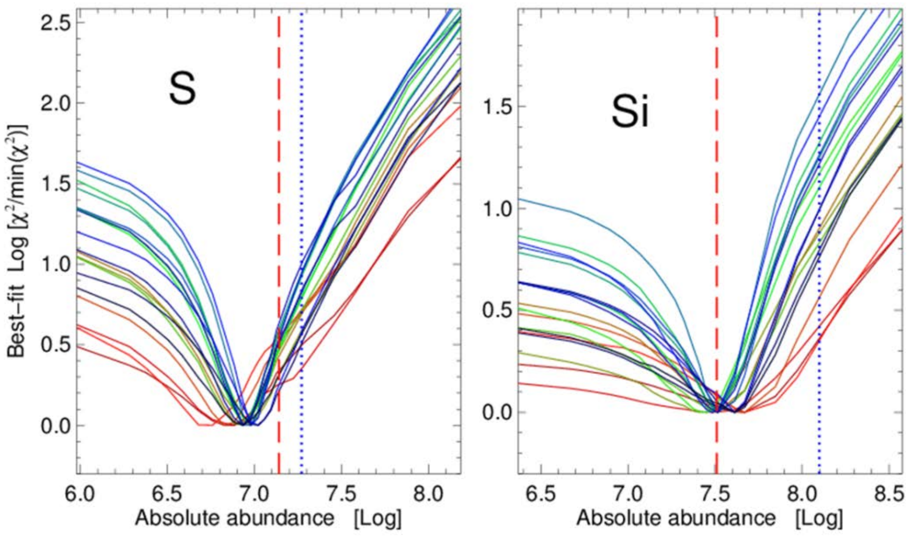

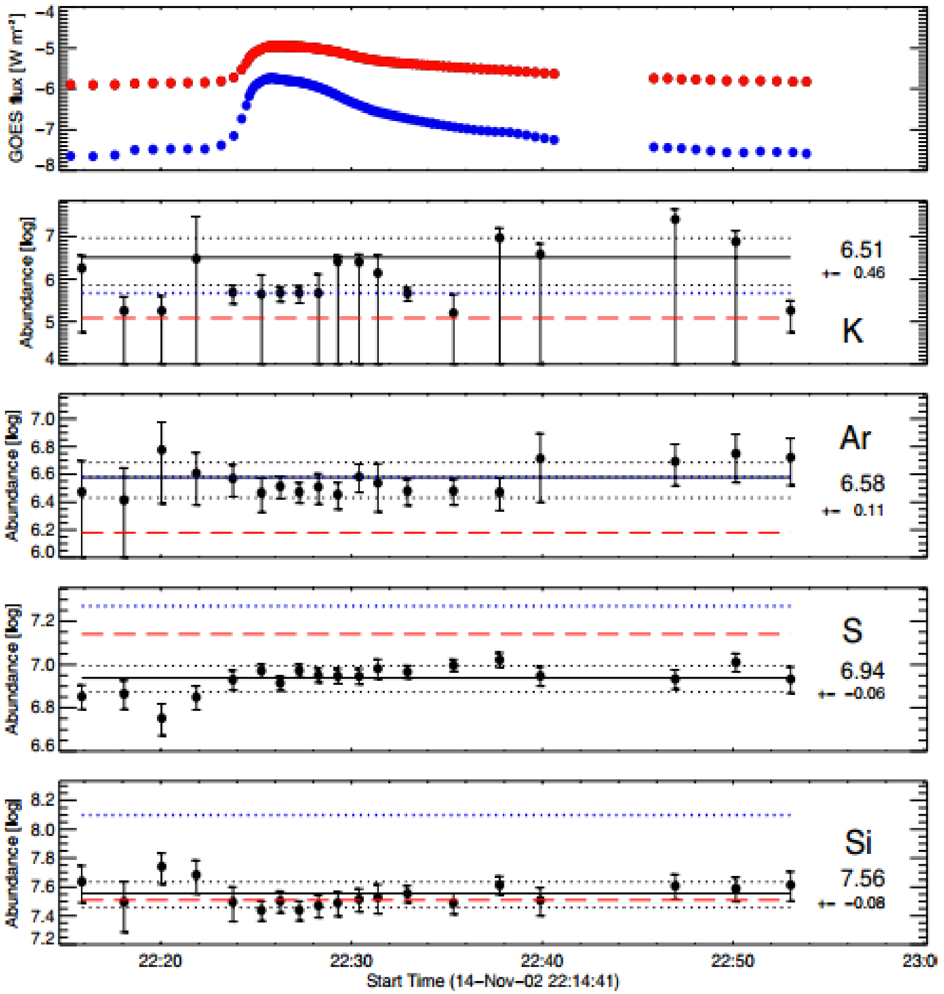

Dashed red line denotes the photospheric and dotted blue the coronal abundance.
Error bars of abundances correspond to values for min(χ^2)+1
Solid black line - time averaged values with rms error bars (dotted)

Further analysis using determined abundances

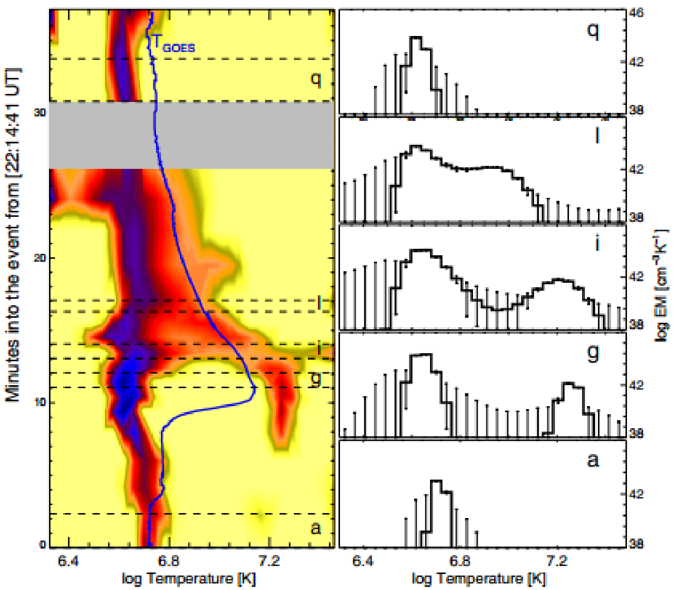

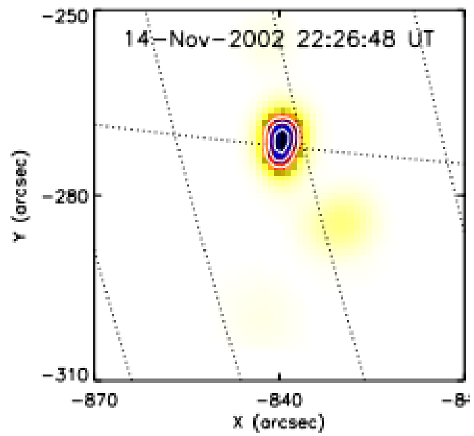

Constant volume based on PIXON reconstructed *RHESSI* 6-7 keV images: 5400 km at 50% iso-contour → hot component parameters (N_e, E_{th})

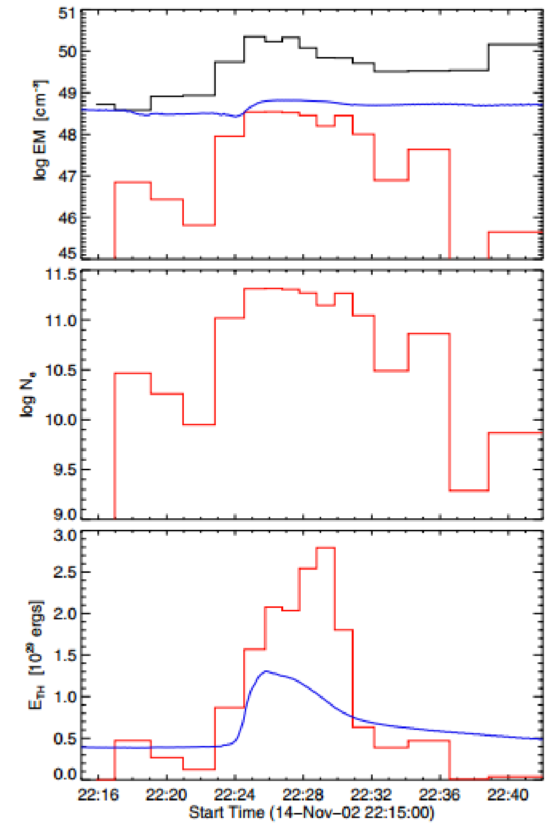

Analysed flares

Data	Time [UT]	Class	Location	Spectra
2003 Jan. 07	07:50	M1.0	S24E08	237
2003 Jan. 07	08:33	C7.7	S12E90	9
2003 Jan. 07	09:15	C1.7	S24E08	21
2003 Jan. 07	11:12	C2.9	S29E92	58
2003 Jan. 07	12:35	C1.3	S15E92	9
2003 Jan. 09	01:39	C9.8	S09W25	292
2002 Nov.14	22:26	M1.0	S15E62	124
2002 Dec.25	18:09	C2.9	S30W91	82
2002 Nov. 12	07:49	C5.3	S12W66	97
2002 Dec. 29	02:05	B9.9	N15W43	34

RESIK data analysed

http://fenyi.sci.klte.hu/DPD/2003/index.html

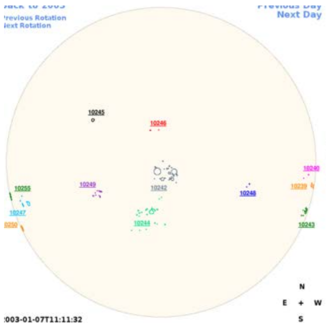

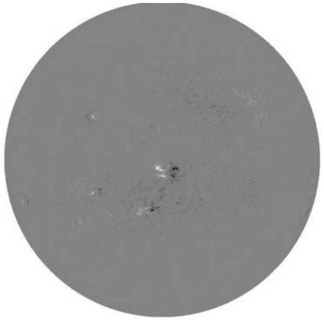

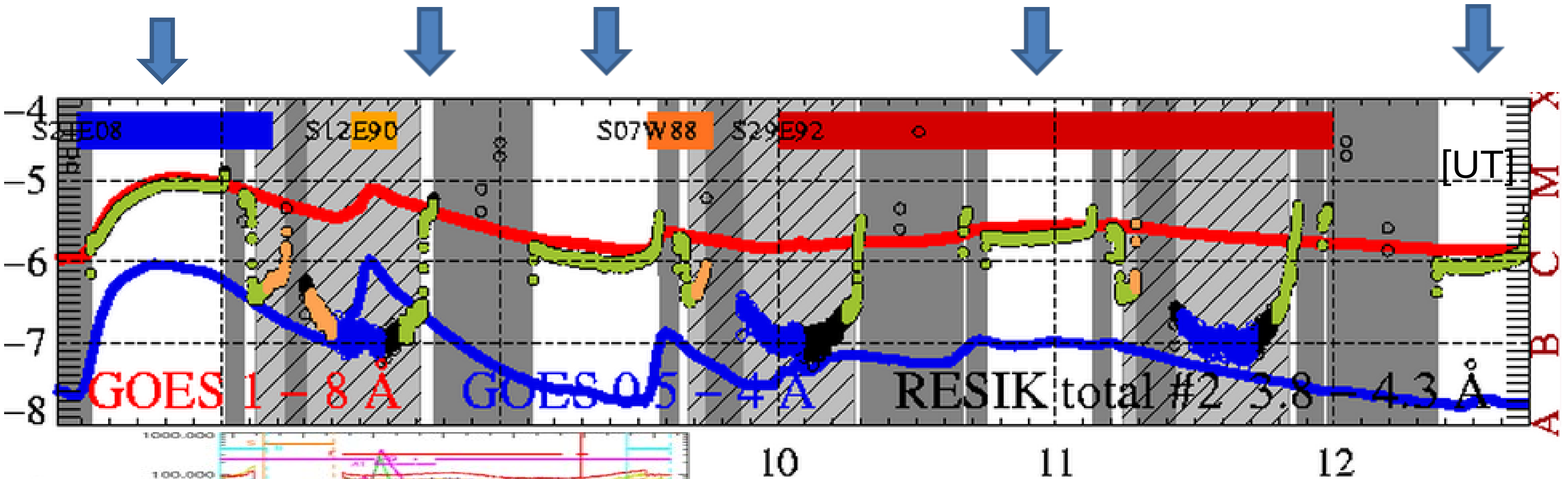

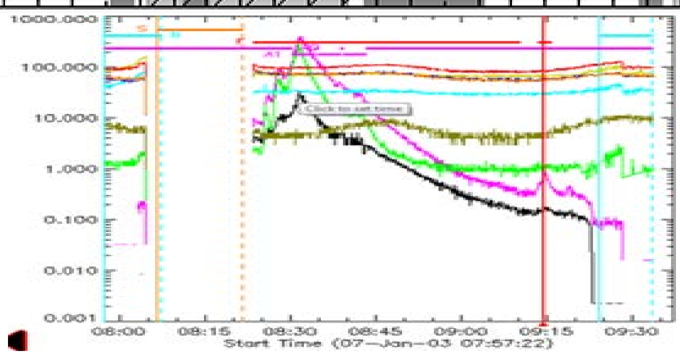

GOES 1-8 Å *GOES* 0.5-4 Å

7 Jan. 2003~07:50 UT

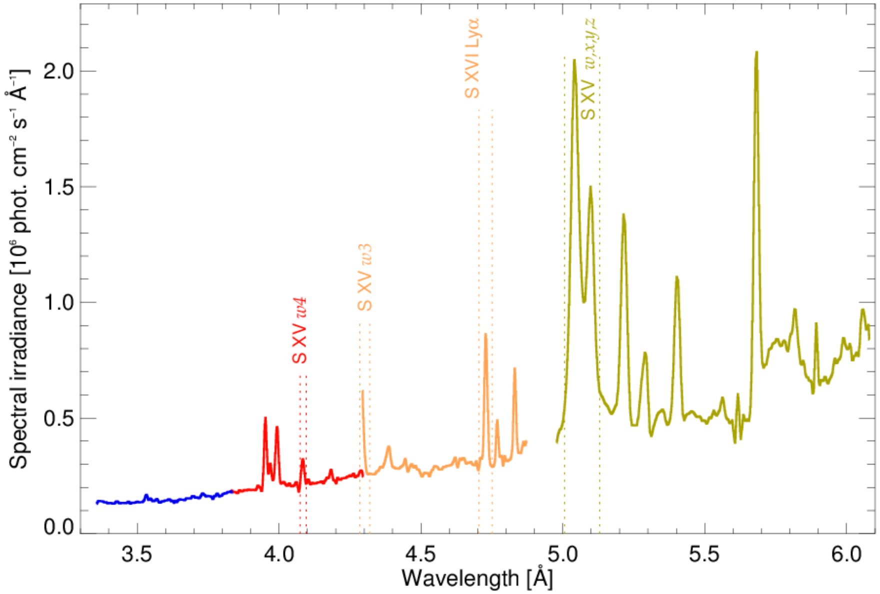

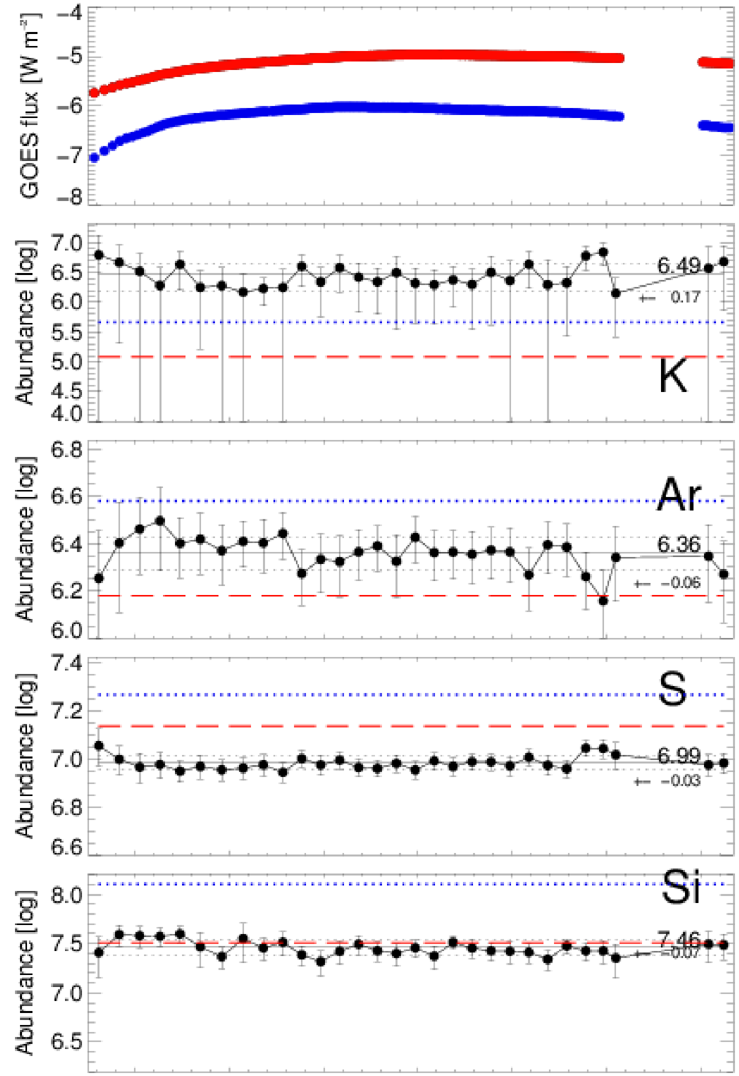

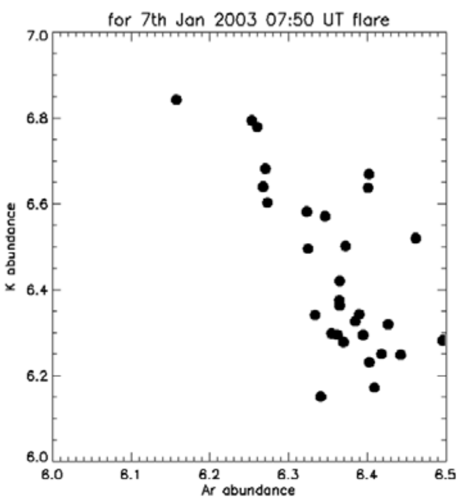

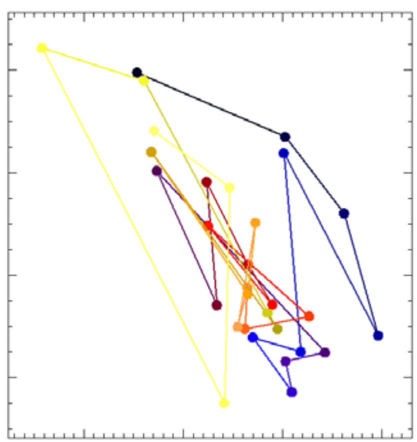

Ar vs K abundance

7 Jan. 2003 : ~08:33 UT   09:15 UT

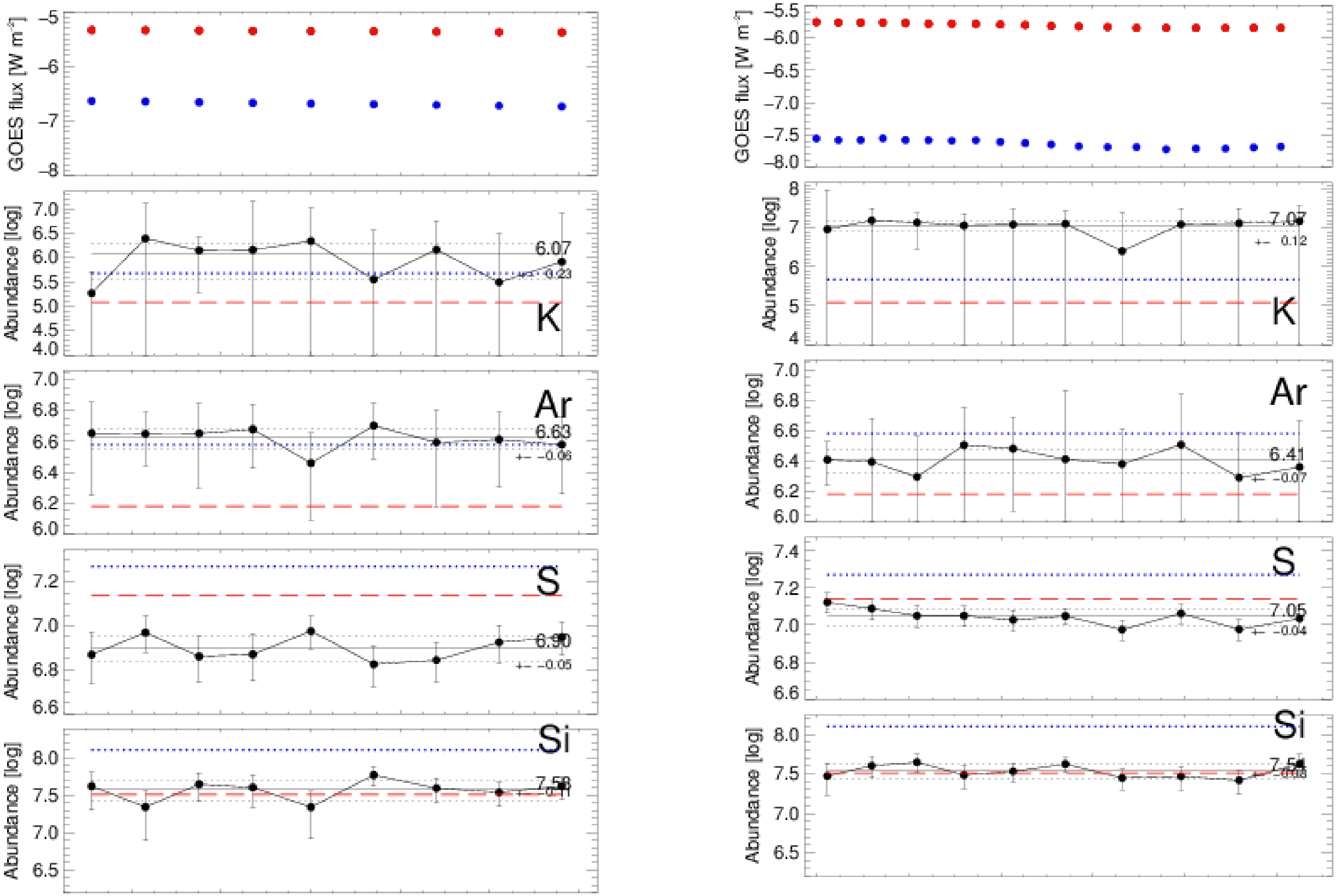

7 Jan. 2003 ~11:12UT

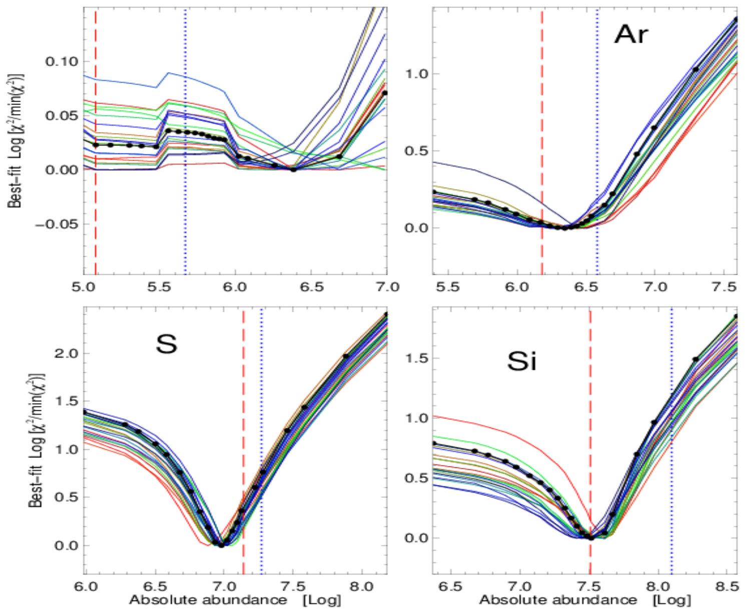

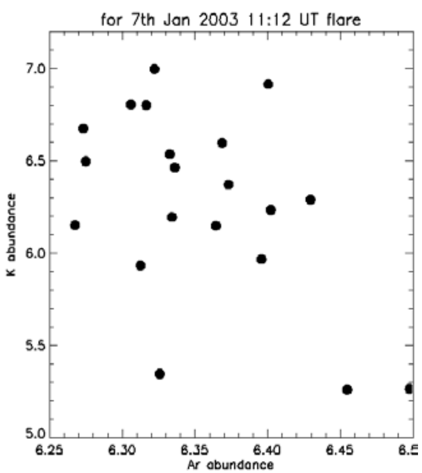

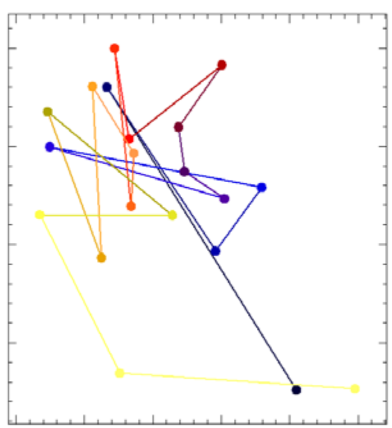

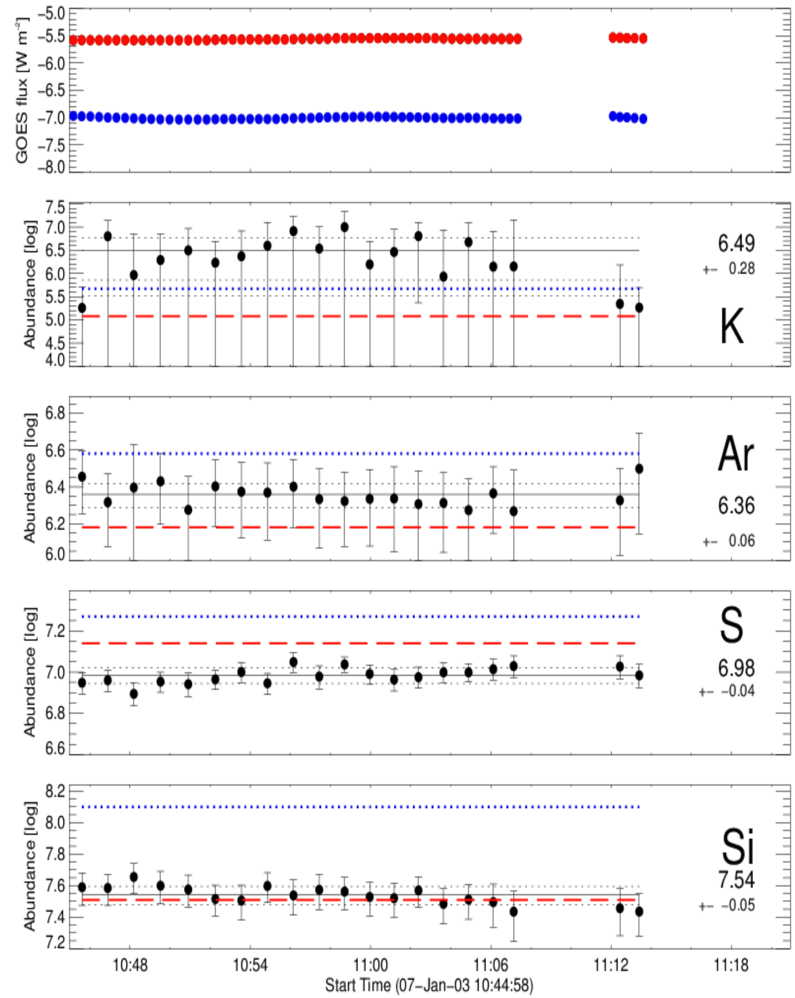

7 Jan. 2003 12:35 UT

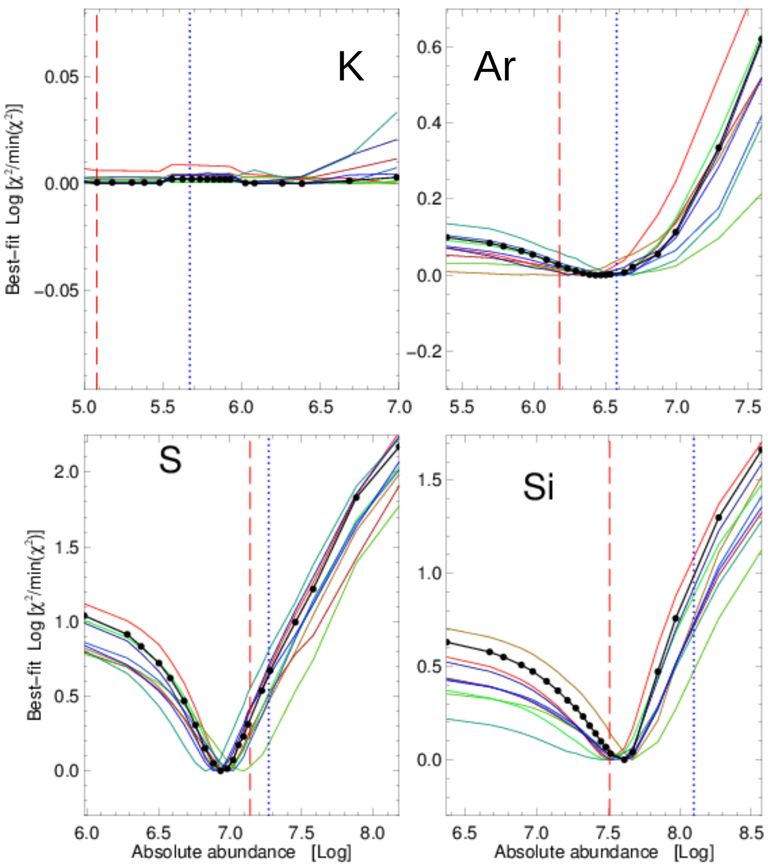

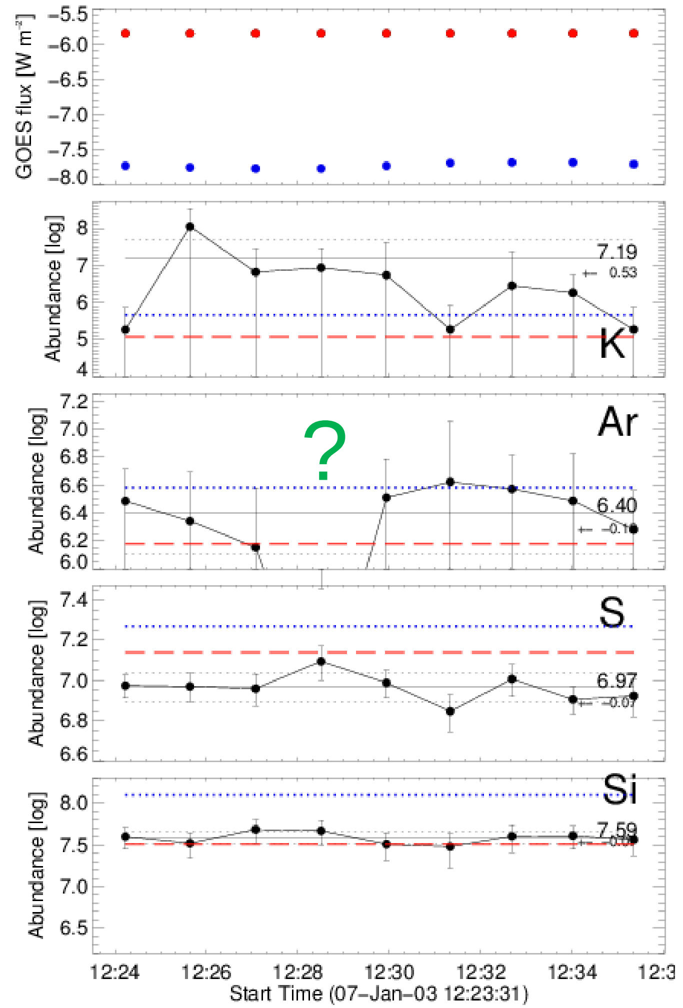

9 Jan 2003 at 01:39 UT; C9.8

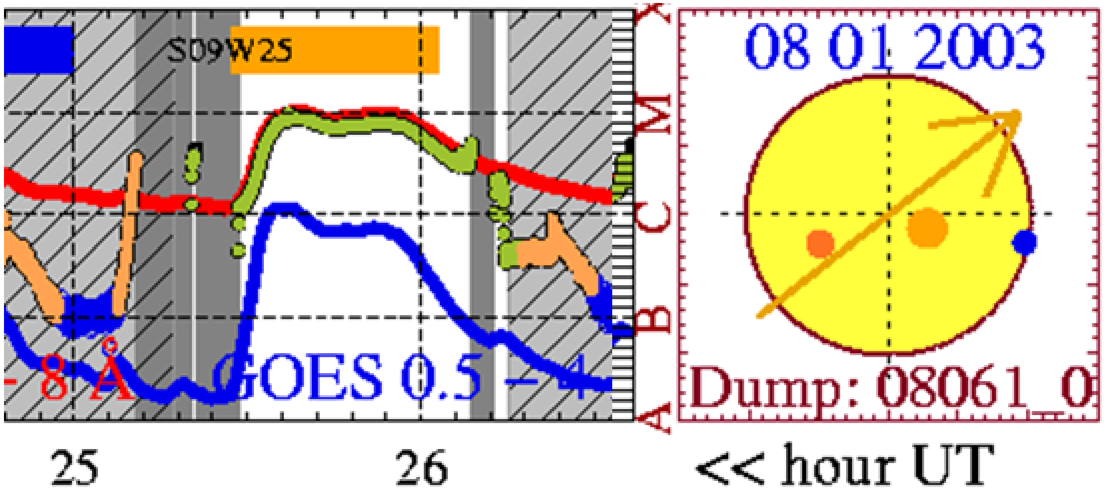

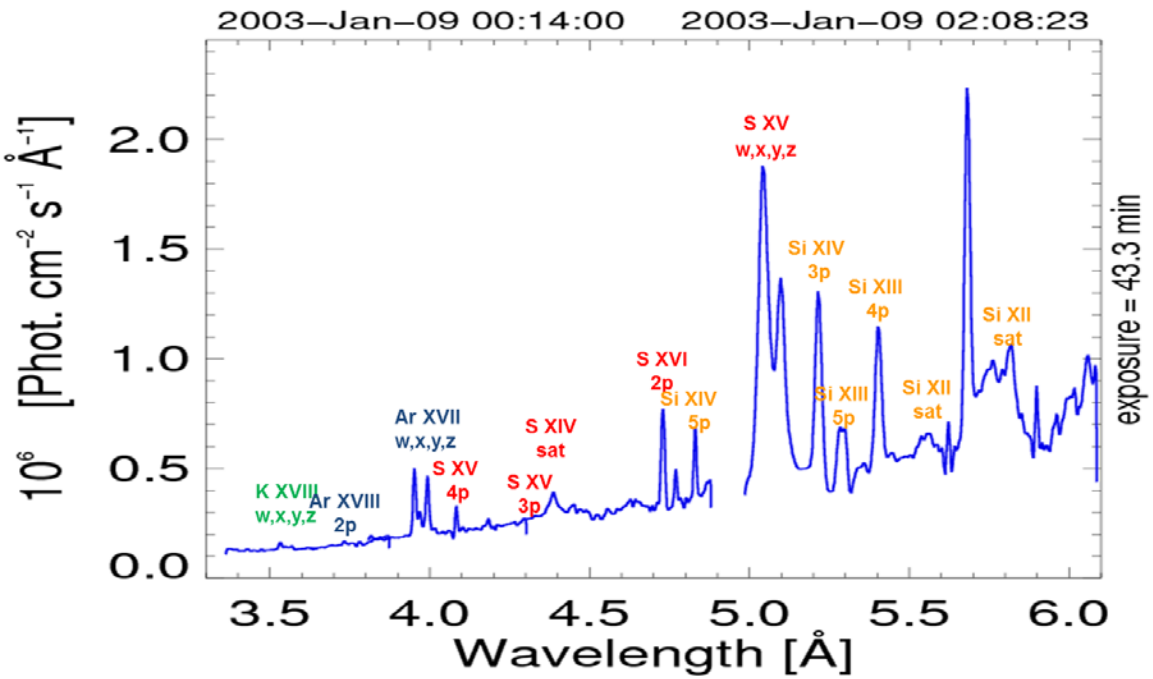

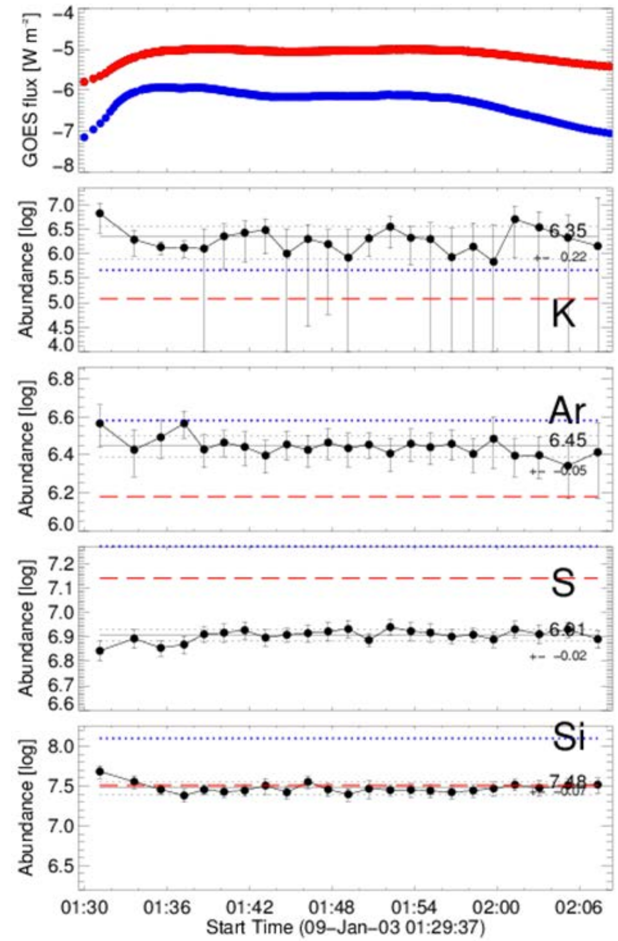

12 Nov. 2002 ~07:49 UT C5.3
25 Dec. 2002 ~18:09 UT C2.9

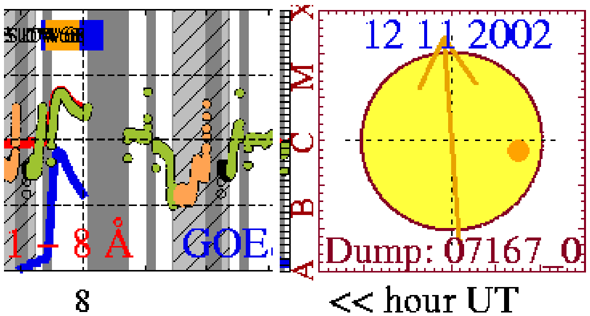

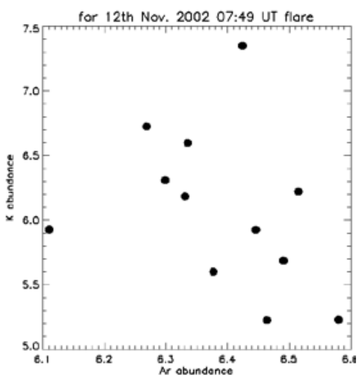

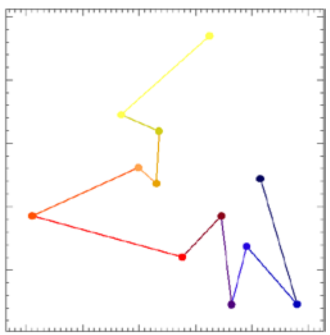

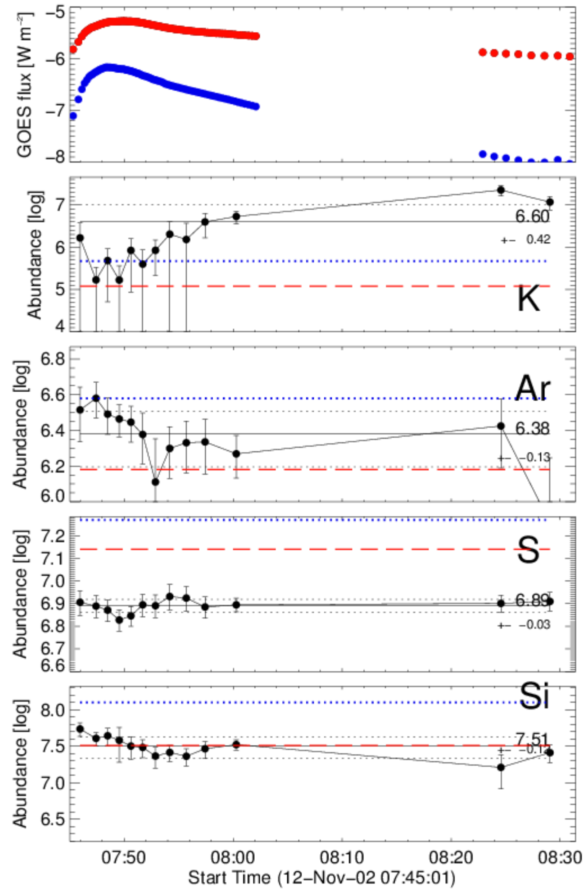

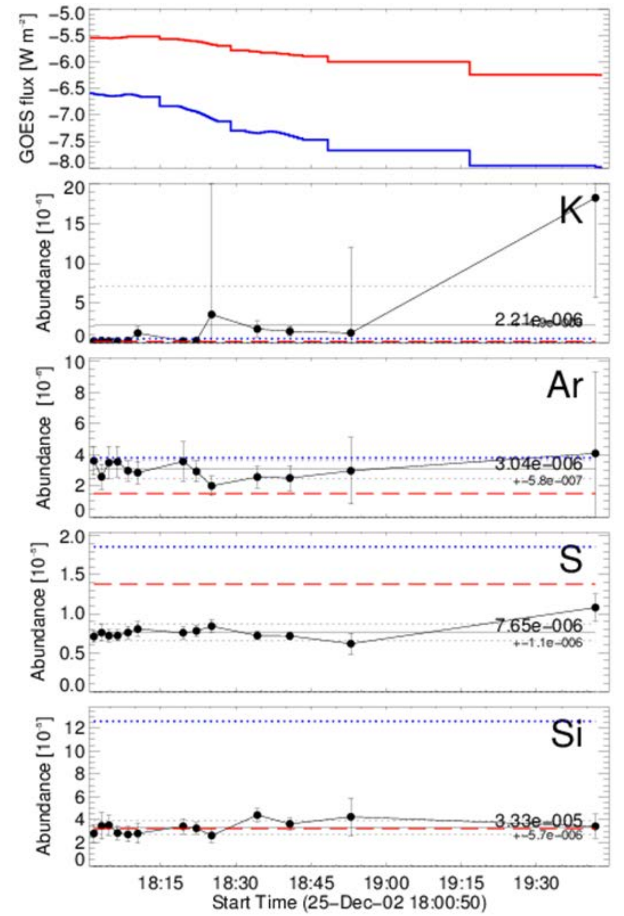

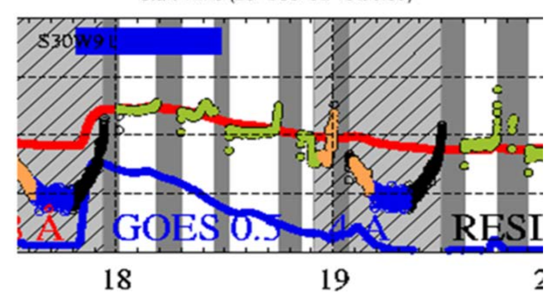

29 Dec. 2002 at 02:05 UT

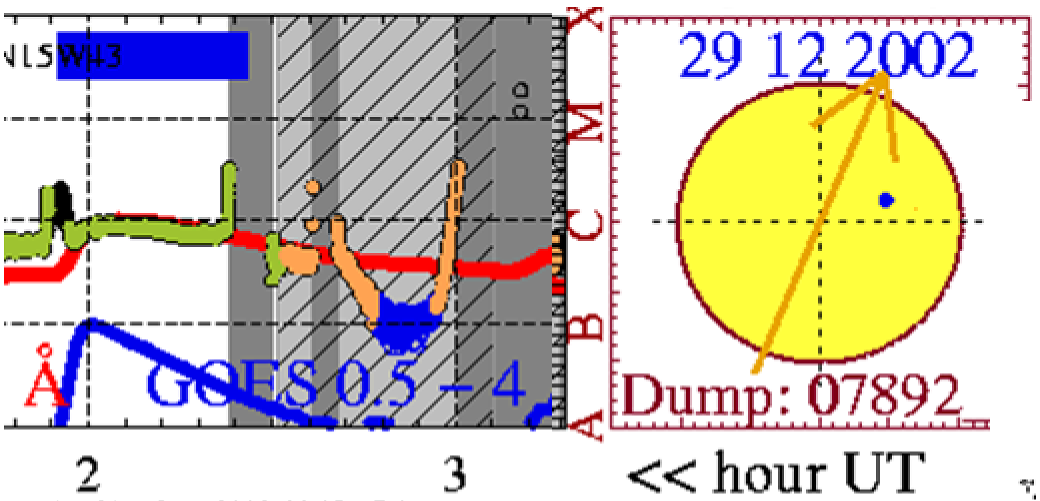

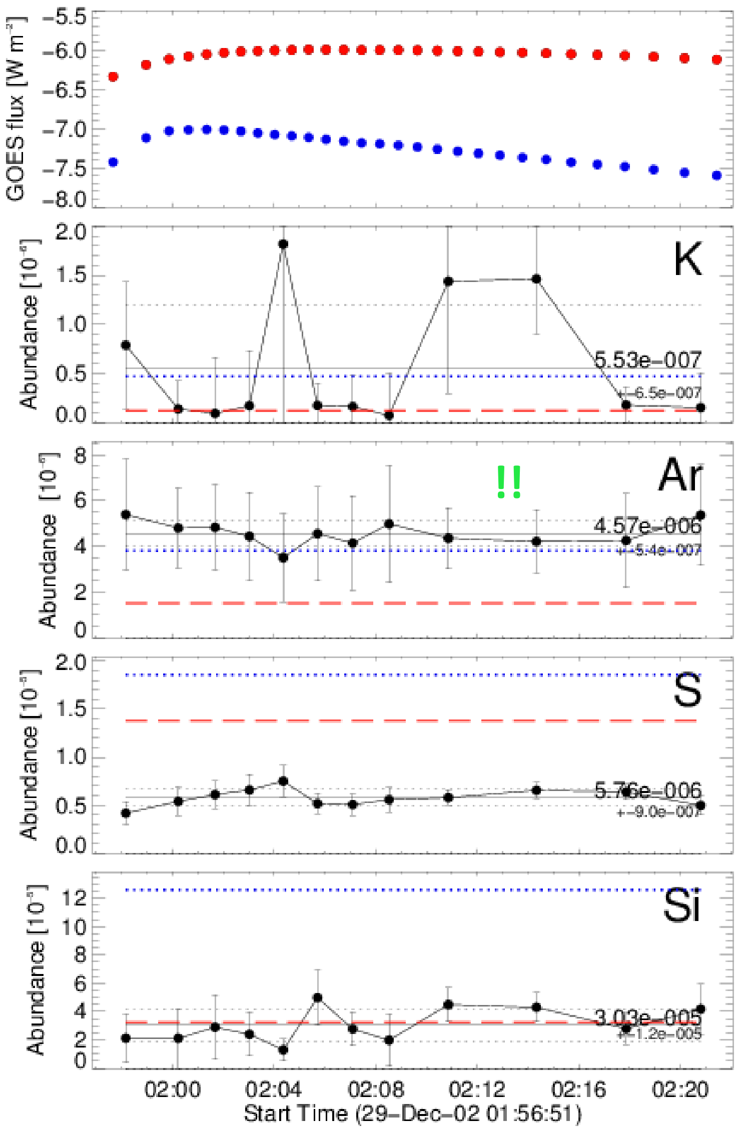

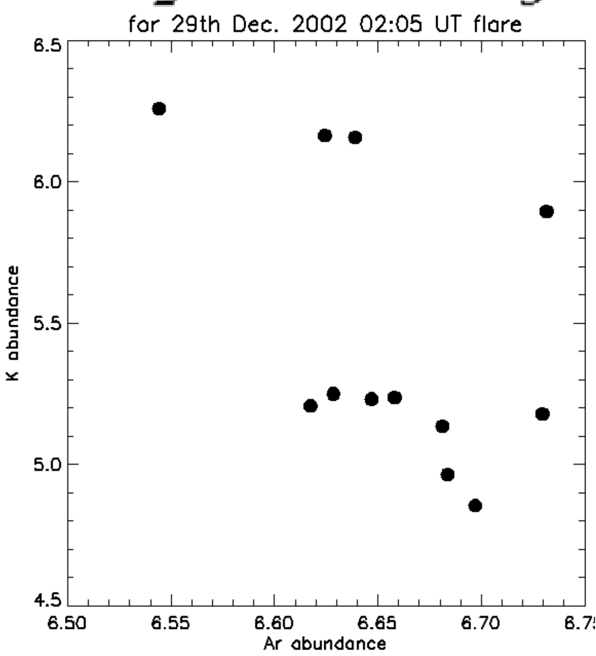

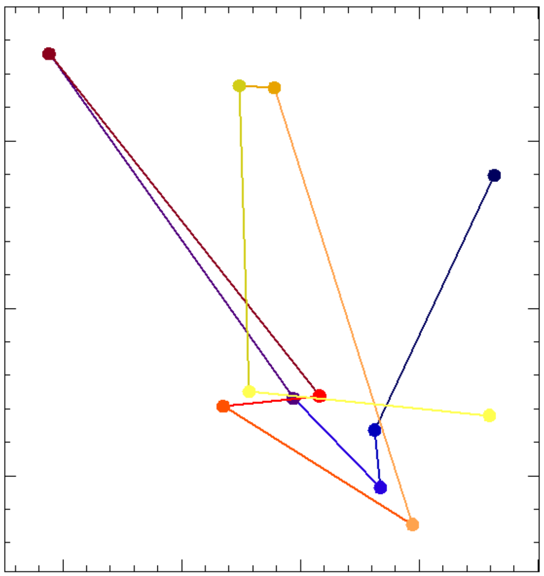

14 Nov. 2002 & All

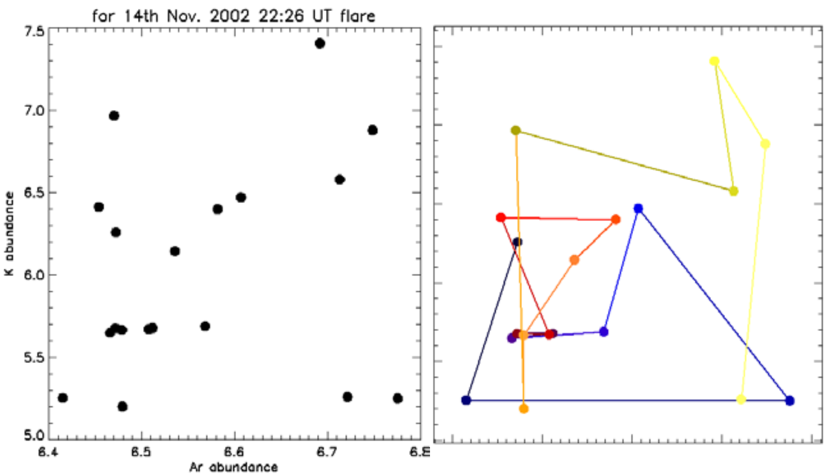

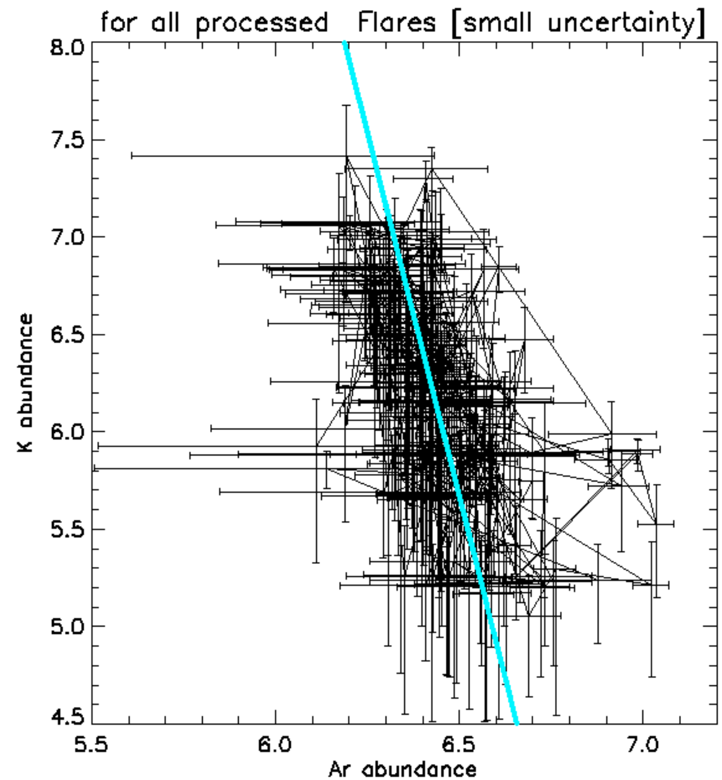

239 przedziałów czasowych (małe błędy; łącznie 634 przedziały)

Observed regularities based on 10 flares

- K (FIP=4.34 eV) abundances usually above coronal value
- Ar (FIP=15.76 eV) abundances always between photospheric and coronal values
- S (FIP=10.36 eV) always below photospheric (inverse FIP effect?)
- Si (FIP=8.15 eV) closed to coronal
- Small changes from flare to flare can be noticed

Plasma composition in a sigmoidal anemone active region

D. Baker, D. H. Brooks, P. Demoulin, L. van Driel-Gesztelyi, L. M. Green, K. Steed, and J. Carlyle; 2013, ApJ, 778, 69

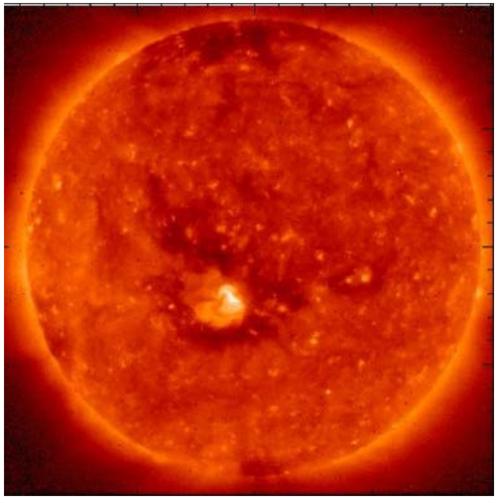

Hinode/XRT Al mesh filter full-disk image for 2007 October 17

***Hinode*/EUV Imaging Spectrometer (EIS)** → detailed spatially resolved abundance map of AR-CH complex (small AR inside low-latitude CH; 359”×485”) based on S X λ=264.223 Å and Si X λ=258.375 Å lines

1. Coaligned intensity images for all spectral lines
2. Fitted Gaussians to strong lines Fe VIII-XVI and S X λ264.223 and Si X λ258.375
3. Determine denisty in each pixel (Fe XIII λ202.044/λ203.826)
4. Calculate contributions functions using CHIANTI with determined density and photospheric abundances assumed
5.Calculating EM distributions using Markov Chain Monte Carlo (MCMC) algorithm and 10 low FIP Fe lines; it should reproduce also Si X intensity (as Si is low FIP)
6. For each pixel convolve EM distributions with contribution functions and fit to the observed intensities to determine the best solution
7. Calculate FIP bias: **ratio of predicted to observed intensity for S X λ264.233 line**

2007 October 17 raster scan at 02:47 UT

Fe XII 195.12 Å

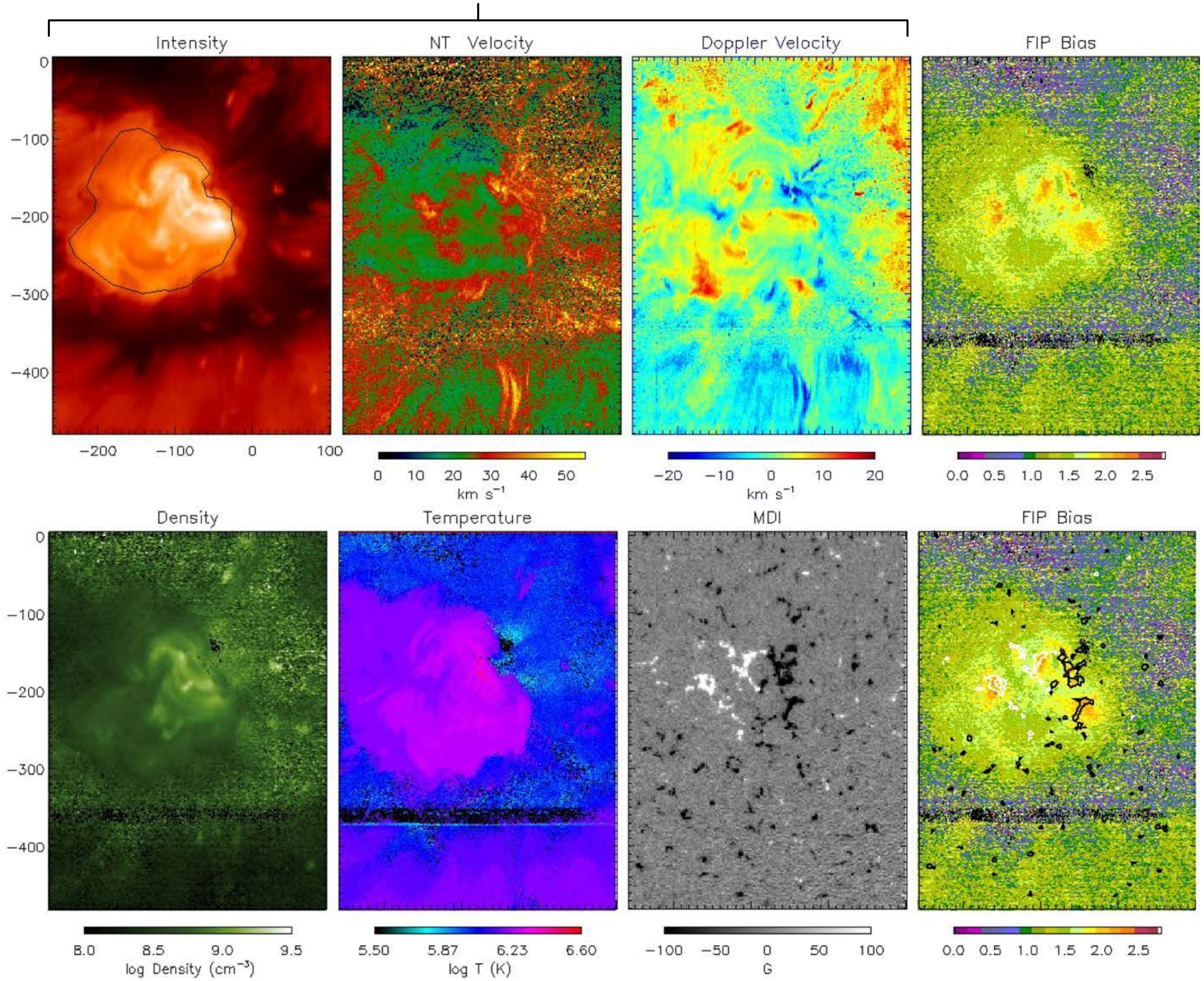

EIS → slit scanning mode: 2" slit, 2" step size, 180 pointing positions each of 45 s exposure time→ FOV 360"×512" during 2¼ hr
EIS Fe XII intensity, nonthermal velocity, Doppler velocity, and abundance maps (S X λ 264.223, Si X λ258.375 and various Fe ions)

EIS Fe XIII density and temperature maps, *SOHO*/MDI magnethogram closest to the EIS raster time and abundance map overlaid with ±100 G MDI contours

Fe XIII λλ 202.02 and 203.83 Å

AR & CH complex; morphological grouping of FIP bias structures

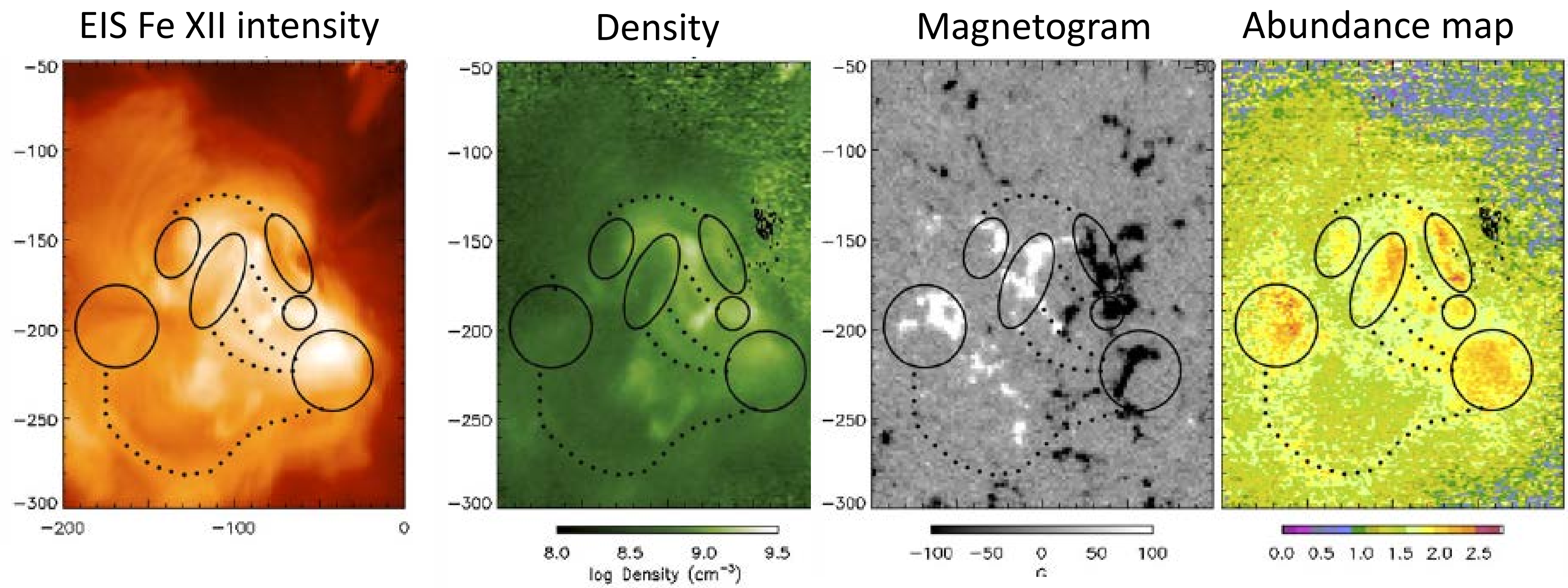

Surrounding CH → photospheric composition (FIP bias=1)
High FIP bias regions (coronal composition) located in a few patches at loops footpoints close to regions of strong magnetic flux (solid black ellipses) and loop traces of enhanced FIP bias (dotted black curves).

Possible links between FIP bias and plasma parameters (correlation plots)

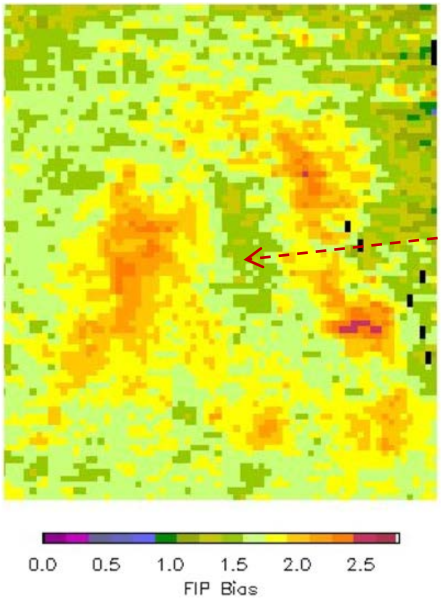

Zoomed abundance map of the inverse S-shaped sigmoid channel of low FIP bias along the main Polarity Inversion Line (PIL) hosting a filament within the AR where a sigmoid/flux rope forms and eventually erupts

Korelacje